

Discovering a hidden binding site of spermidine synthase inhibitors for Chagas disease by combining molecular simulations and X-ray crystallography

Ryunosuke Yoshino^{2,4}, Nobuaki Yasuo^{1,4}, Yohsuke Hagiwara^{4,5}, Takashi Ishida^{3,4}, Daniel Ken
Inaoka^{6,7}, Yasushi Amano⁵, Yukihiro Tateishi⁵, Kazuki Ohno^{4,5}, Ichiji Namatame⁵, Tatsuya
Niimi⁵, Masaya Orita⁵, Kiyoshi Kita^{6,7}, Yutaka Akiyama^{1,3,4}, Masakazu Sekijima^{1,4*}

¹ School of Computing, Tokyo Institute of Technology, 4259-J3-23, Nagatsuta-cho, Midori-
ku, Yokohama, Japan

² Transborder Medical Research Center, University of Tsukuba, 1-1-1 Tenodai, Tsukuba, Ibaraki,
305-8577, Japan

³ School of Computing, Tokyo Institute of Technology, Meguro-ku, Tokyo 152-8550, Japan

⁴ Education Academy of Computational Life Sciences (ACLS), Tokyo Institute of Technology,

19 Yokohama 226-8501 Japan

20

21 ⁵ Medicinal Chemistry Research Labs, Drug Discovery Research, Astellas Pharma Inc, 21

22 Miyukigaoka, Tsukuba, Ibaraki 305-8585 Japan

23

24 ⁶ Department of Biomedical Chemistry, Graduate School of Medicine, The University of Tokyo,

25 Bunkyo-ku, Tokyo, 113-0033, Japan

26

27 ⁷ School of Tropical Medicine and Global Health, Nagasaki University, Sakamoto, Nagasaki,

28 852–8523, Japan

29

30 *Corresponding author

31 E-mail: sekijima@c.titech.ac.jp

32

Abstract

Background

Chagas disease is caused by the parasite *Trypanosoma cruzi* and is one of the neglected tropical diseases. Although two types of drugs are currently available, new drugs are still required because they have serious side effects. To develop a therapeutic agent for trypanosomiasis, we focused on spermidine synthase (SpdSyn) as the target protein and determined the hidden binding site which was not identified in the X-ray structure for obtaining seed compounds using a computational simulation.

Methodology/Principal Findings

Molecular dynamics (MD) simulation was performed for TcSpdSyn to predict new binding sites. These results indicated that the highly druggable binding site was discovered around Glu22. We also conducted docking simulation for the new binding site and in vitro assay to determine half-maximal inhibitory concentration (IC_{50}) value. Furthermore, to confirm ligand of binding site and pose, we conducted X-ray crystallographic studies. As a result, two compounds were discovered as inhibitors of TcSpdSyn with IC_{50} values of 82.27 and 43.41 μM , respectively. X-ray crystallographic analysis shows that two inhibitors are bound to the hidden binding site which is detected by computational simulation.

51

52 **Conclusions/Significance**

53 MD simulation revealed that there are new sites in the TcSpdSyn that are not an active site.

54 This site exists near Glu22 and Asp77, and crystal structures revealed that compounds **1** and

55 **2** are bound to the hidden binding site, as predicted by MD simulations, and interacts with

56 Glu22 and Asp77 through hydrogen bonds. 4MCHA which has been reported as known

57 inhibitor binds to the TcSpdSyn active site while interacting with Asp171. Therefore, these

58 inhibitors we discovered differs in binding mode from a known inhibitor and this new binding

59 site is useful for antitrypanosomiasis target.

60

61 Keywords: Chagas disease, Trypanosomes, Spermidine synthase, Molecular dynamics, In

62 silico screening

63 **Author Summary**

64 Predicting the binding site of a target protein is very important in drug design. Computational

65 methods, such as machine learning and molecular dynamics (MD), are effective for these

66 predictions. In this study, we predicted a new drug-binding site on spermidine synthase from

67 *Trypanosoma cruzi* (TcSpdSyn) using MD simulations. In addition, we performed docking

68 simulations to search for new seed compounds and conducted in vitro enzyme assays to

determine the IC₅₀ value. From these results, a new binding site, which was not identified in the X-ray structure, was predicted. We identified two hit compounds that inhibit TcSpdSyn by *in silico* and *in vitro* screening. Moreover, we confirmed the structure of the complexes of TcSpdSyn with these hit compounds by X-ray analysis. These TcSpdSyn–inhibitor complex structures demonstrated that the hit compounds bind to the site predicted by the MD simulations.

Introduction

Chagas disease, which is classified as a neglected tropical disease, is caused by the parasite *Trypanosoma cruzi* (*T. cruzi*) [1,2]. Nifurtimox and benznidazole, two current treatments for Chagas disease, have serious side effects and limited effectiveness during the chronic phase of Chagas disease [3-5]. Thus, the demand for new therapeutic treatments for Chagas disease is high.

Drug discovery is generally expensive and time-consuming, requiring approximately \$2.6 billion dollars and 12–14 years for a drug to reach the market [6]. Computational methods offer a way of reducing these barriers to drug discovery, development and design. Drug design processes are divided into two types. Ligand-based drug design (LBDD) is based on activity values (such as half-maximal inhibitory concentration, IC₅₀), and known compound

properties involved in drug binding. Representative methods in LBDD are quantitative structure-activity relationship (QSAR) studies and machine learning. Alternatively, structure-based drug design (SBDD) bases the design process on a target protein structure. In SBDD, discovery of the target protein binding site is a fundamental starting point [6,7]. Typically, the protein binding site is identified by X-ray analysis and the drug is designed or optimized based on information from that analysis. Human immunodeficiency virus 1 (HIV-1) protease inhibitors were developed using SBDD [8-10]. Thus, binding site information, such as shape and physical properties, are very important for drug development and optimization.

Drugs that bind to proteins, such as enzymes, are roughly divided into two types: competitive inhibitors and noncompetitive inhibitors. Competitive inhibitors bind to active sites at which the protein catalyzes a reaction. In contrast, noncompetitive inhibitors bind to nonactive sites, such as allosteric sites. Non-competitive inhibitors that bind to allosteric sites have several advantages compared with competitive inhibitors that bind to active sites, including low side effects and high affinities [11]. Thus, the determination of new binding site such as allosteric sites is important in drug development studies. Yet, although all proteins are potentially allosteric [12], few cases of allosteric inhibitors have been reported.

To detect binding site for drug design, computational methods to identify binding sites, such as POCKET [13], LIGSITE [14], CAST [15], PASS [16] and SURFNET [17], have been

reported. These methods estimate the protein binding site from the three-dimensional geometry of the protein, and no ligand is required. Moreover, several studies have adopted machine learning methods, such as the support vector machine (SVM) method, for predicting allosteric sites [18-20]. Virtual screening methods, such as protein–ligand docking simulations [21], have been applied in computational binding site identification studies.

Computer-aided drug discovery has been applied to develop new drugs. Protein–ligand docking simulations, such as DOCK [22,23], AutoDock [24], GOLD [25] and Glide [26,27] are the most frequently used virtual screening methods, whereas molecular dynamics (MD) simulations are used to collect protein-ligand complex ensembles [28] in SBDD. Many successful virtual screening studies have been reported [29-40]. Moreover, pharmacophore [41] modeling studies using protein–ligand complex structures have also been reported [42,43]. Typically, traditional computational methods, such as binding site identification and protein–ligand docking simulations, do not take into account protein flexibility, because the calculations are for a single point. Therefore, the results from these methods depend on the initial protein structure. By contrast, MD simulations account for protein flexibility using Newtonian principles. Ma et al. reported a computational method for predicting allosteric sites from residue–residue interaction patterns [44]. In that study, conformational ensembles of a target protein generated by MD simulations for site prediction were applied. Thus, MD

simulations can used for identifying new binding sites and ligand binding poses that traditional computational methods cannot.

In this study, we discovered a new binding site for *T. cruzi* spermidine synthase (TcSpdSyn), as an antitrypanosomiasis target [45-50], and used MD simulations and conduct docking simulations to identify anti-Chagas drug candidates that binds to the new site. We then performed in vitro assays to determine the inhibition activities of compounds identified by the docking simulations, and performed subsequent X-ray crystallographic studies of the active compounds. Finally, we conducted fragment molecular orbital (FMO) calculations to analyze important interactions between TcSpdSyn and the active compounds.

Methods

Computational Methods

The structure of TcSpdSyn (PDB ID: 3BWC), as the docking target, was obtained from the Protein Data Bank. The hydrogenation, water removal, and conformation optimization of the complex were accomplished in Maestro using the OPLS2005 force field [51]. And carboxyl group of S-adenosylmethionine (SAM) which is included in the structure was deleted to correct SAM to Decarboxylated S-adenosylmethionine (dcSAM) as a cofactor. The MD simulation system was prepared using Desmond ver. 3.5 with the default settings. The

temperature and pressure of the system were set to 300 K and 1 atm, respectively. The time step and structure sampling interval were set to 2 fs and 1 ps, respectively. We performed the simulation five times under the NPT ensemble for 20 ns. Next, we merged all trajectories from the MD simulation and performed structure clustering based on the amino acid residues at active site, which are shown in the Table S1, using average linkage in AMBER [52]. After clustering, site volume and druggability of the active center were evaluated by SiteMap [53].

Docking simulations were performed at the active site of the prepared structure in the absence of the natural substrate putrescine. For the docking simulation, a $20 \times 20 \times 20 \text{ \AA}^3$ grid box was generated, thereby maintaining the TcSpdSyn active site. dcSAM, as a cofactor, was not deleted. We used Glide in standard precision (SP) mode [26, 27] for our docking simulations of approximately 4,800,000 drug-like compounds in the Namiki Sho-ji Co., Ltd., library and the Astellas Pharma Inc. in-house compound library that satisfy Lipinski's rule of five [54]. All calculations were performed on an HP Proliant SL390s G7 server with an Intel Xeon X5670 2.93 GHz core and five nodes on the TSUBAME2.5 supercomputer at the Tokyo Institute of Technology.

The X-ray crystallography structures of TcSpdSyn with compounds **1** and **2** were hydrogenated in Maestro using the OPLS2005 force field. FMO calculation input files were generated using FMOutil Version 2.1, and calculations were performed for the TcSpdSyn

complexes with **1** and **2** using GAMESS [55] at the MP2/6-31G level. Interaction energy analysis was performed using the analytical tool Facio [56], which is based on pair interaction energy decomposition analysis, as proposed by Fedorov and Kitaura [57].

***In vitro* Assay**

The protocol for the TcSpdSyn inhibition assay has been described previously [58]. The assay was performed using an enzyme-coupled assay incorporating spermidine/spermine N(1)-acetyltransferase (SSAT1). 7-Diethylamino-3-(4'-maleimidylphenyl)-4-methylcoumarin (cat. D-346, Thermo Fischer Scientific) was used to measure coenzyme A produced from the SSAT1 reaction. Briefly, a reaction mixture of 4-(2-hydroxyethyl)-1-piperazineethanesulfonic acid (HEPES) buffer (50 mM, pH 7.5) containing ethylenediaminetetraacetic acid (EDTA, 10 μ M), 0.01% Tween 20, TcSpdSyn (14.7 nM), dcSAM (50 μ M), putrescine (50 μ M), acetyl coenzyme A (15 μ M), and SSAT1 (0.83 nM) in the presence or absence of **1** or **2** was incubated at room temperature for 30 min. The concentrations of putrescine and dcSAM were determined using their K_m values (data not shown). The fluorescence signals were detected using a Paradigm plate reader (Molecular Devices) with excitation at 405 nm and emission at 530 nm. IC_{50} values were calculated from dose-response curves in which each of eight data points represents the average of four

measurements (S2 Fig). Compound 2 was used as the hydrochloride salt. These compounds were dissolved in dimethyl sulfoxide (DMSO), the final concentration of which in the assays was as high as 1.3%.

X-ray crystallography analysis

The protocol for X-ray crystallography has been described previously [58]. Briefly, co-crystals of TcSpdSyn complexed with dcSAM and compound **1** were obtained using the sitting-drop vapor diffusion method. Prior to crystallization, TcSpdSyn (15 mg/mL) was mixed with dcSAM and compound **1** at final concentrations of 2 and 5 mM, respectively. A reservoir solution consisting of bis-Tris (100 mM, pH 5.5–6.5), ammonium sulfate (200 mM), and 10–15% (w/v) PEG4000 was prepared. The precipitated crystals were transferred into a mother liquor containing 20% (v/v) glycerol as a cryoprotectant, which was then flash frozen in liquid nitrogen. X-ray diffraction data were collected at the Photon Factory (Tsukuba, Japan) AR-NE3A beamline using a robotic sample changer and an automated data collection system [59,60]. The structure was resolved by molecular replacement using Phaser [61]. The apo-structure of TcSpdSyn (PDB ID: 3BWB) was used as a reference model. After structural refinement using REFMAC [62], dcSAM and compound **1** were clearly observed in the electron density maps and fitted to the maps using AFITT (OpenEye Scientific). The final

structures were deposited in the Protein Data Bank (PDB IDs: 5Y4P and 5Y4Q).

Results

Discovering of hidden binding by molecular dynamics

To predict TcSpdSyn binding sites, we performed MD simulations and structure clustering for virtual screening. S1 Fig in the Supporting Information shows the root-mean-square deviations (RMSD) of TcSpdSyn α -carbon atoms, side chains and heavy atoms during a 20 ns MD simulation. Next, we conducted structure clustering to extract representative structures from the trajectory. Fig 1 shows the active site of TcSpdSyn in the X-ray structure and clustering structures.

Fig 1. TcSpdSyn target site in the X-ray and clustering structures. A: X-ray structure (volume: 193 Å³, D-score: 0.56), B: clustering structure 1 (volume: 496 Å³, D-score: 1.12, population: 0.178)

The active site volume of the X-ray structure was 193 Å³. However, the active site volumes of the clustering structures were 496 Å³. In clustering structure 1 (Fig 1B), a new cavity, which was not identified in the X-ray structure, was discovered around Glu22. Furthermore, the D-

scores indicating druggability of the clustering structures were higher than that of the X-ray structure. Target sites with D-score higher than 0.98 are highly druggable [53]. These results suggest that the target site of TcSpdSyn is flexible and has a structure with higher druggable potentially. It is possible that compounds which are not found in the case of using the X-ray structure are evaluated by using the predicted structure. And we suggested that molecules that inhibit structural change can bind to the new site. We defined the new site as a hidden binding site and then performed docking simulations for the hidden binding sites in the clustering structures. And we also performed docking simulations for active site in the X-ray structure to compare docking simulation results between hidden binding sites and active site in the X-ray structure. Fig1

In silico screening by docking study

To obtain drug candidates from our combined library of 4,800,000 drug-like compounds, we conducted docking simulations for the TcSpdSyn hidden binding site, as predicted by MD simulations and active site in the X-ray structure, using Glide in the SP mode. Fig 2 shows the docking poses of the top five compounds with high docking score at each binding site.

Fig 2. Comparison of docking poses of the top five compounds with high docking score at each binding site. A: docking pose of the X-ray structure, B: docking pose of the

clustering structure. Stick model shows Glu22 and dcSAM, and line model shows docking results.

The X-ray docking results show that these compounds bind to the TcSpdSyn active center, which is adjacent to dcSAM. In contrast, the docking poses in the clustering structures cover a wide range of hidden binding sites. Fig 3 shows the diversity of top 10,000 compounds with high docking scores in each docking results.

Fig 3. Docking results depending on the presence of heterocycle and/or chiral centers.

A: results of the X-ray structure, B: results of clustering structure 1.

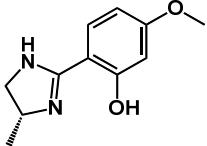
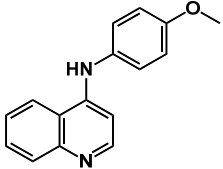
In the X-ray structure (Fig 3A), many compounds lacking a heterocycle or chiral center are favored. In contrast, more compounds containing a heterocycle and/or chiral center are favored with clustering structure 1 (Fig 3B). Overall, our docking simulations identified a variety of compounds after performing MD simulations and structure clustering.

In vitro assay and X-ray crystallography analysis

We ran docking simulations targeted to the “virtual” hidden binding site found in the MD

simulations. Next, we selected 191 compounds among the docking results for hidden binding site and performed *in vitro* enzyme assay to validate their IC₅₀ concentration value. The results showed that two compounds exhibited inhibitory activity (Table 1).

Table 1. Summary of TcSpdSyn inhibition by compounds 1 and 2. PDB IDs for the co-crystallized enzyme–inhibitor complexes, IC₅₀ values, and the molecular structures of the inhibitors.

	PDB ID	IC ₅₀ (μM)	Compound structure
Compound 1	5Y4P	82.27	
Compound 2	5Y4Q ^a	43.41	

^aSalt form with HCl

To examine the binding sites used by these two active compounds, we conducted X-ray crystallographic studies to observe the structures of the TcSpdSyn complex with the two top-ranked compounds (compounds 1 and 2) in the hidden binding pocket (Fig 4), as predicted by the MD simulations.

262

263 **Fig 4. Binding site of each compound confirmed by X-ray analysis.** A: TcSpdSyn with
264 compound 1 (5Y4P), B: TcSpdSyn with compound 2 (5Y4Q).

265

266 These data show that compound **1** interacts with Glu22 and Asp77 through hydrogen bonding
267 (Fig 4A). Compound **2** interacts with Glu22 and Asp77, similar to **1**, and the lone pair of the
268 quinoline nitrogen atom in **2** is proximal to the carboxylate group of Glu22. Thus, these results
269 suggest that Glu22 is in a neutral state when interacting with the lone pair of quinoline.

270 Next, we conducted an interaction energy analysis for each X-ray structure using FMO
271 calculations. Fig 5A shows the results of the interaction energy analysis of the TcSpdSyn–**1**
272 complex.

273

274 **Fig 5. Interaction energy analysis of each X-ray structure.** A: interaction energy of
275 compound **1**, B: interaction energy of compound **2**. C: interaction energy of cis-4-
276 methylcyclohexanamine (4MCHA, PDBID: 2PT9). The y-axis represents the interaction
277 energy (kcal/mol) between the ligand and each amino acid residue, and the x-axis represents
278 the amino acid residue number.

279

Compound **1** interacts with Glu22 and Asp77 (interaction energy values: -25.93 and -17.56 kcal/mol, respectively) through two hydrogen bonds. Therefore, these interactions would appear to be important for binding to the site. Some other interactions were also found: Trp61, Ile71, Thr244, and Tyr245 interacted with compound **1** with interaction energies of -4.45, -6.51, -4.83, and -7.36 kcal/mol, respectively. Fig 5B shows the results of the interaction energy analysis of the TcSpdSyn-**2** complex. Compound **2** interacted with Glu22 and Asp77 (interaction energy values: -20.08 and -30.05 kcal/mol, respectively) through two hydrogen bonds in the same manner as **1**. In particular, Asp77 interacted with compound **2** in a neutral state. Moreover, some weak interactions, such as with Ile71 Tyr245 and Ile247, were confirmed, with interaction energy values of -7.16, -6.96, and -5.71 kcal/mol, respectively. Fig 5C shows the results of the interaction energy analysis of the TcSpdSyn-cis-4-methylcyclohexanamine (4MCHA) complex (PDB ID: 2PT9) [63]. 4MCHA has been reported as known inhibitor and binds to the TcSpdSyn active site [63]. This inhibitor interacted with Asp171 (interaction energy: -14.29 kcal/mol). Furthermore, 4MCHA also interacted with dcSAM which is cofactor of SpdSyn. These results suggested that compound **1** and **2** shows interaction pattern different from 4MCHA.

Fig 6 shows the amino acid sequence of the binding sites defined by LIGSITE^{csc} [64].

Fig 6. Amino acid residue sequence of the binding sites. X-ray: sequence of the TcSpdSyn–**1** complex (5Y4P), MD: sequence of the clustering structure identified from the MD simulations. The residue was determined using yellow at the binding site. A binding site is defined as a residue within 10 Å of an atom defined by LIGSITE^{csc}.

Upon examination of the X-ray structure of TcSpdSyn with compound **1** at the binding site, the amino acid sequence overlap with the clustering structure was 72.2%. Glu22, which interacts with **1**, is a feature of the sequence of the clustering structure binding site. Therefore, the MD simulations predicted the new binding site of TcSpdSyn and the amino acid residue that contributes a significant interaction at the binding site.

Discussion

Using a molecular simulation approach, we conducted MD simulations to predict new TcSpdSyn binding sites. These MD simulations suggest a new binding site that was not evident in the X-ray structure. The binding site predicted by MD simulations shows a higher D-score and larger volume than the X-ray structure. This binding site appears from structural changes in the protein.

To obtain seed compounds for potential anti-Chagas drugs, we performed docking

simulations using the TcSpdSyn X-ray structure and clustering structures. These simulations identified active compounds from approximately 4,800,000 drug-like compounds. In accordance with the X-ray structure, drug candidates lacking a heterocycle and chiral center were considered. In contrast, drug candidates containing a heterocycle and/or chiral center were considered for clustering structure 1, as predicted from the MD simulations. Thus, docking simulations combined with MD simulations can evaluate a variety of compounds.

To evaluate their IC₅₀ values, drug candidates from the docking results were screened in TcSpdSyn inhibition assays. As a result, TcSpdSyn IC₅₀ values for two compounds were determined. Compounds **1** and **2** showed TcSpdSyn inhibition with IC₅₀ values of 82.27 and 43.41 μM, respectively. Furthermore, to confirm the binding mode, we determined the X-ray structure of the TcSpdSyn–ligand complexes. The crystal structures revealed that compounds **1** and **2** are bound to the hidden binding site, as predicted by the simulations, and interacts with Glu22 and Asp77 through hydrogen bonds. These hydrogen bonds are not observed in the TcSpdSyn active site structure to which putrescine is bound. Thus, the hidden binding site predicted by MD simulations is a new target site that has not been previously reported.

Comparing the structures of compound **1** and **2**, both compounds are *para*-substituted anisoles and both *para*-substituents are nitrogen-rich heterocycles. However, the X-ray

structures show opposite orientations for compound **1** and **2** in the new site. Compound **1** interacts with Glu22 through the hydroxy group at *meta*-position of anisoles. In contrast, compound **2** interact with Glu22 through a secondary amine at para substituent. Accordingly, two compounds show different poses despite including a common structure.

This hidden binding site discovered by this research is located next to the active site and known inhibitor binding to the active site of TcSpdSyn has been reported such as 4MCHA. Furthermore, we also have reported inhibitors binding to the active site of TcSpdSyn [65]. To improve inhibitory activity of these compounds for TcSpdSyn, it is possible to design compounds binding to both sites based on results of this study. These results could possibly facilitate the development of new compound for TcSpdSyn-targeted anti-Chagas drugs. And this virtual screening method, using docking simulations and MD simulations, could be invaluable for drug discovery.

Acknowledgment

This research was partially supported by the Platform Project for Supporting Drug Discovery and Life Science Research (Basis for Supporting Innovative Drug Discovery and Life Science Research (BINDS)) from AMED under Grant Number JP20am0101112, Japanese Society for the Promotion of Science (JSPS) KAKENHI Grant Numbers

20H00620 (to M.S.) and 16J09021 (to N.Y.).

References

[1] Lockman JW, Hamilton AD. Recent developments in the identification of

chemotherapeutics for Chagas disease. *Curr Med Chem*. 2005;12(8):945-959.

[2] Hayley EM, Anna O, Kim P, Susan CW. Neglected zoonotic diseases-the long and

winding road to advocacy. *PLoS Negl Trop Dis*. 2014;8(6):e2800. doi:

10.1371/journal.pntd.0002800.

[3] Farrar J, Hotez PJ, Junghanss T, Gagandeep K, Lalloo D, White N. Trypanosomiasis:

Chagas Disease. In: Peter JH, Thomas J, Ga-gandeep K, editors. *Reviews in Man-son's*

Tropical Infectious Diseases 23. Toronto: Elsevier; 2013. p. 622–630.

[4] Plum XM. Chagas' disease—an epidemic that can no longer be ignored. *The Lancet*.

2006;368(9536):619.

[5] Carlos AM, Jose AM, Alvaro A, Sergio S, Anis R, Fernando R, et al. Randomized Trial of

Benznidazole for Chronic Chagas' Cardiomyopathy. *N Engl J Med*. 2015;373(14):1295-

1306.

[6] Ringe D. What makes a binding site a binding site? *Curr Opin Struct Biol*.

1995;5(6):825-829.

370 [7] Ruppert J, Welch W, Jain AN. Automatic identification and representation of protein
371 binding sites for molecular docking. *Protein Sci.* 1997;6(3):524-533.

372 [8] Rutenber E, Fauman EB, Keenan RJ, Fong S, Furth PS, Montellano PRO, et al.
373 Structure of a non-peptide inhibitor complexed with HIV-1 protease. Developing a cycle of
374 structure-based drug design. *J Biol Chem.* 1993;268(21):15343–15346.

375 [9] Ghosh AK, Thompson WJ, Fitzgerald PMD, Culberson JC, Axel MG, et al. Structure-
376 Based Design of HIV-1 Protease Inhibitors: Replacement of Two Amides and a 10.pi.-
377 Aromatic System by a Fused Bis-tetrahydrofuran. *J Med Chem.* 1994;37(16):2506–2508.

378 [10] Lam PYS, Jadhev PK, Eyermann CJ, Hodge CN, Ru Y, et al. Rational design of potent,
379 bioavailable, nonpeptide cyclic ureas as HIV protease inhibitors. *Science.*
380 1994;263(5145):380–384.

381 [11] Peracchi A, Mozzarelli A. Exploring and exploiting allostery: Models, evolution, and
382 drug targeting. *Biochim Biophys Acta.* 2011;1814(8):922–933.

383 [12] Gunasekaran K, Ma B, Nussinov R. Is allostery an intrinsic property of all dynamic
384 proteins? *Proteins.* 2004;57:433–443.

385 [13] Levitt DG, Banaszak LJ. POCKET: a computer graphics method for identifying and
386 displaying protein cavities and their surrounding amino acids. *J Mol Graph.* 1992;10:229-
387 234.

388 [14] Hendlich M, Rippmann F, Barnickel G. LIGSITE: automatic and efficient detection of
389 potential small molecule-binding sites in proteins. *J Mol Graph Model*. 1997;15(6):359-363.

390 [15] Liang J, Edelsbrunner H, Woodward C. Anatomy of protein pockets and cavities:
391 measurement of binding site geometry and implications for ligand design. *Protein Sci*.
392 1998;7(9):1884-1897.

393 [16] Brady GP, Stouten PF. Fast prediction and visualization of protein binding pockets with
394 PASS. *J Comput Aided Mol Des*. 2000;14(4):383-401.

395 [17] Laskowski RA. SURFNET: a program for visualizing molecular surfaces, cavities, and
396 intermolecular interactions. *J Mol Graph*. 1995;13(5):323-330.

397 [18] Demerdash ON, Daily MD, Mitchell JC. Structure-based predictive models for allosteric
398 hot spots. *PLoS Comput Biol*. 2009;5(10):e1000531. doi: 10.1371/journal.pcbi.1000531.
399 Epub 2009 Oct 9.

400 [19] Guilloux V, Schmidtke P, Tuffery P. BMC Bioinf. Fpocket: An open source platform for
401 ligand pocket detection. 2009;10:168.

402 [20] Huang W, Lu S, Huang Z, Liu X, Mou L, Luo Y, et al. Allosite: a method for predicting
403 allosteric sites. *Bioinformatics*. 2013;29(18):2357–2359.

404 [21] Ivan TB, Woody S, Matt R, Thijs B. Improved docking of polypeptides with Glide. *J*
405 *Chem Inf Model*. 2013;53(7):1689–1699.

406 [22] Kuntz ID, Blaney JM, Oatley SJ, Langridge R, Ferrin TE. A geometric approach to
407 macromolecule-ligand interactions. J Mol Biol. 1982;161(2):269–288.

408 [23] Ewing TJ, Makino S, Skillman AG, Kuntz ID. DOCK 4.0: search strategies for
409 automated molecular docking of flexible molecule databases. J Comput Aided Mol Des.
410 2001;15(5):411–428.

411 [24] Morris GM, Goodsell DS, Halliday RS, Huey R, Hart WE, Belew RK, et al. J Comput
412 Chem. 1998;19:1639–1662.

413 [25] Jones G, Willett P, Glen RC, Leach AR, Taylor R. Development and validation of a
414 genetic algorithm for flexible docking. J Mol Biol. 1997;267(3):727–748.

415 [26] Friesner RA, Banks JL, Murphy RB, Halgren TA, Klicic JJ, Mainz DT. et al. Glide: a new
416 approach for rapid, accurate docking and scoring. 1. Method and assessment of docking
417 accuracy. J Med Chem. 2004;47(7):1739–1749.

418 [27] Halgren TA, Murphy RB, Friesner RA, Beard HS, Frye LL, Pollard WT, et al. Glide: a
419 new approach for rapid, accurate docking and scoring. 2. Enrichment factors in database
420 screening. J Med Chem. 2004;47(7):1750–1759.

421 [28] Lin JH, Perryman AL, Schames JR, McCammon JA. Computational Drug Design
422 Accommodating Receptor Flexibility: The Relaxed Complex Scheme. J Am Chem Soc.
423 2002;124:5632-5633.

424 [29] Kuntz ID. Structure-Based Strategies for Drug Design and Discovery. *Science*.
425 1992;257:1078–1082.

426 [30] Babine RE, Bender SL. Molecular Recognition of Protein–Ligand Complexes:
427 Applications to Drug Design. *Chem Rev*. 1997;97:1359–1472.

428 [31] Jorgensen WL, The Many Roles of Computation in Drug Discovery. *Science*.
429 2004;303:1813–1818.

430 [32] Muegge I, Rarey M. Small molecule docking and scoring. In: Lipkowitz KB, Boyd DB,
431 editors. *Reviews in Computational Chemistry*. Hoboken: Wiley-VCH; 2001. p. 1–60.

432 [33] Böhm HJ, Stahl M. The use of scoring functions in drug discovery applications. In:
433 Lipkowitz KB, Boyd DB, editors. *Reviews in Computational Chemistry*. Hoboken: Wiley-
434 VCH; 2002. p. 41–88.

435 [34] Brooijmans N, Kuntz ID. Molecular recognition and docking algorithms. *Annu Rev*
436 *Biophys Biomol Struct*. 2003;32:335–373.

437 [35] Schulz-Gasch T, Stahl M. Scoring functions for protein-ligand interactions: a critical
438 perspective. *Drug Discovery Today*. 2004;1(3):231–239.

439 [36] Kitchen DB, Decornez H, Furr JR, Bajorath J. *Nat Rev Drug Discovery*.
440 2004;3(11):935–949.

441 [37] Leach AR, Shoichet BK, Peishoff CE. Prediction of Protein–Ligand Interactions.

442 Docking and Scoring: Successes and Gaps. *J Med Chem.* 2006;49(20):5851–5855.

443 [38] Shuntaro C, Kazuyoshi I, Takashi I, Michael G, Y-h T, Mitsuo I, et al. Identification of
444 potential inhibitors based on compound proposal contest: Tyrosine-protein kinase Yes as a
445 target. *Scientific Reports.* 2015;5:17209. doi: 10.1038/srep17209.

446 [39] Shuntaro C, Takashi I, Kazuyoshi I, Masahiro M, Reiji T, Y-h T, et al. An iterative
447 compound screening contest method for identifying target protein inhibitors using the
448 tyrosine-protein kinase Yes. *Scientific Reports.* 2017;7:12038. doi: 10.1038/s41598-017-
449 10275-4.

450 [40] Nobuaki Y, and Masakazu S. Improved Method of Structure-Based Virtual Screening
451 via Interaction-Energy-Based Learning. *J Chem Inf Model.* 2019;59:1050-1061. doi:
452 10.1021/acs.jcim.8b00673.

453 [41] Wermuth CG, Ganellin CR, Lindberg P, Mitscher LA. Glossary of terms used in
454 Medicinal chemistry. *Pure and Applied Chemistry.* 1998;70:1129–1143.

455 [42] Catherine JL, Boon HT. Pharmacophore-based screening targeted at upregulated FN1,
456 MMP-9, APP reveals therapeutic compounds for nasopharyngeal carcinoma. *Computers in*
457 *Biology and Medicine.* 2016;69:158–165.

458 [43] Ryunosuke Y, Nobuaki Y, Daniel KI, Yohsuke H, Kazuki O, Masaya O, et al.
459 Pharmacophore modeling for anti-Chagas drug design using the fragment molecular orbital

method. PLoS One. 2015;10(5):e0125829. doi: 10.1371/journal.pone.0125829.

[44] Ma X, Qi Y, Lai L. Allosteric sites can be identified based on the residue–residue interaction energy difference. *Proteins*. 2015;83(8):1375–1384.

[45] Ariyanayagam MR, Oza SL, Guthrie ML, Fairlamb AH. Phenotypic analysis of trypanothione synthetase knockdown in the African trypanosome. *Biochem J*. 2005;391(Pt 2):425-432.

[46] Huynh TT, Huynh VT, Harmon MA, Phillips MA. Gene knockdown of gamma-glutamylcysteine synthetase by RNAi in the parasitic protozoa *Trypanosoma brucei* demonstrates that it is an essential enzyme. *J Biol Chem*. 2003;278(41):39794-39800.

[47] Krieger S, Schwarz W, Ariyanayagam MR, Fairlamb AH, Krauth-Siegel RL, Clayton C. Trypanosomes lacking trypanothione reductase are avirulent and show increased sensitivity to oxidative stress. *Mol Microbiol*. 2000;35(3):542-252.

[48] Li F, Hua SB, Wang CC, Gottesdiener KM. *Trypanosoma brucei brucei*: characterization of an ODC null bloodstream form mutant and the action of alpha-difluoromethylornithine. *Exp Parasitol*. 1998;88(3):255-257.

[49] Taylor MC, Kaur H, Blessington B, Kelly JM, Wilkinson SR. Validation of spermidine synthase as a drug target in African trypanosomes. *Biochem J*. 2008;409(2):563-569.

[50] Willert EK, Phillips MA. Regulated expression of an essential allosteric activator of

polyamine biosynthesis in African trypanosomes. PLoS Pathog. 2008;4(10):e1000183. doi:
10.1371/journal.ppat.1000183.

[51] George AK, Richard AF, Julian TR, William LJ. Evaluation and Reparametrization of
the OPLS-AA Force Field for Proteins via Comparison with Accurate Quantum Chemical
Calculations on Peptides. J Phys Chem. 2001;105(28):6474-6487.

[52] Jianyin S, Stephen WT, Nephi T, Thomas EC. Clustering Molecular Dynamics
Trajectories: 1. Characterizing the Performance of Different Clustering Algorithms. J Chem
Theory Comput. 2007;3(6):2312–2334.

[53] Thomas AH. Identifying and characterizing binding sites and assessing druggability. J
Chem Inf Model. 2009;49(2):377–389.

[54] Christopher AL, Franco L, Beryl WD, Paul JF. Experimental and computational
approaches to estimate solubility and permeability in drug discovery and development
settings. Adv Drug Deliv Rev. 2001;46(1-3):3-26.

[55] Michael WS, Kim KB, Jerry AB, Steven TE, Mark SG, Jan HJ, et al. General atomic
and molecular electronic structure system. J Comput Chem. 1993;14:1347-1363.

[56] Suenaga M. Facio: New Computational Chemistry Environment for PC GAMESS.
Journal of Computer Chemistry Japan. 2005;4(1):25-32.

496 [57] Fedorov DG, Kitaura KJ. Pair interaction energy decomposition analysis. J Comput
497 Chem. 2007;28(1):222-237.

498 [58] Amano Y, Namatame I, Tateishi Y, Honboh K, Tanabe E, Niimi T, et al. Structural
499 insights into the novel inhibition mechanism of Trypanosoma cruzi spermidine synthase.
500 Acta Crystallogr D Biol Crystallogr. 2015;71(Pt 9):1879-1889.

501 [59] Hiraki M, Watanabe S, Honda N, Yamada Y, Matsugaki N, Igarashi N, et al. High-
502 throughput operation of sample-exchange robots with double tongs at the Photon Factory
503 beamlines. J Synchrotron Radiat. 2008;15(Pt 3):300-303.

504 [60] Hiraki M, Yamada Y, Chavas LM, Wakatsuki S, Matsugaki NJ. Improvement of an
505 automated protein crystal exchange system PAM for high-throughput data collection. J
506 Synchrotron Radiat. 2013;20(Pt 6):890-893.

507 [61] McCoy AJ, Grosse-Kunstleve RW, Adams PD, Winn MD, Storoni LC, Read RJ. Phaser
508 crystallographic software. J Appl Crystallogr. 2007;40(Pt 4):658–674.

509 [62] Murshudov GN, Vagin AA, Dodson EJ. Refinement of macromolecular structures by
510 the maximum-likelihood method. Acta Crystallogr D Biol Crystallogr. 1997;53(Pt 3):240-255.

511 [63] Dufe VT, Qiu W, Müller IB, Hui R, Walter RD, Al-Karadaghi S. Crystal structure of
512 Plasmodium falciparum spermidine synthase in complex with the substrate decarboxylated
513 S-adenosylmethionine and the potent inhibitors 4MCHA and AdoDATO. J Mol Biol.

514 2007;373(1):167-177.

515 [64] Bingding H, Michael S. LIGSITEcsc: predicting ligand binding sites using the Connolly
516 surface and degree of conservation. BMC Struct Biol. 2006;6:19.

517 [65] Ryunosuke Y, Nobuaki Y, Yohsuke H, Takashi I, Daniel KI, Yasushi A, et al. In silico, in
518 vitro, X-ray crystallography, and integrated strategies for discovering spermidine synthase
519 inhibitors for Chagas disease. Scientific Reports. 2017;7(1):6666. doi: 10.1038/s41598-
520 017-06411-9.

521

522 **Supporting information**

523 **S1 Fig. Root-mean-square deviations (RMSD) in the MD simulations.** Blue: α -carbon,
524 gray: side chains, yellow: heavy atoms.

525 **S2 Fig. The fitting curves for the calculation of the IC₅₀ values in Table 1 (A:**
526 **compound 1, B: compound 2).** The error bars represent the standard error of the %
527 inhibition measured at each dose.

528 **S1 Table. Reference of amino acid residues for structure clustering.**

529 **S2 Table. Crystallography data for the TcSpdSyn–1 and TcSpdSyn–2 complexes.**

530 **S3 Table. SMILES of inactive compounds.**